Materials Transactions, Vol. 47, No. 3 (2006) pp. 845 to 848

Microstructure Characterization and Mechanical Properties of $TiSi_2$–SiC–Ti_3SiC_2 Composites Prepared by Spark Plasma Sintering

Chao Qin[1,2], Lianjun Wang[1], Wan Jiang[1], Shengqiang Bai[1] and Lidong Chen[1,*]

[1]*State Key Laboratory of High Performance Ceramics and Superfine Microstructure, Shanghai Institute of Ceramics, Chinese Academy of Sciences, 1295 Dingxi Road, Shanghai 200050, P. R. China*
[2]*Graduate School of Chinese Academy of Sciences, Beijing, P. R. China*

Dense $TiSi_2$–SiC and $TiSi_2$–SiC–Ti_3SiC_2 composites in which SiC particles in 200–300 nm disperse, were reactively synthesized through spark plasma sintering (SPS) technique using TiC, Si, and C powders in micrometer as starting reactants. The phase constituents and microstructures of the samples were analyzed by X-ray diffraction, field emission scanning electron microscopy and transmission emission microscopy. The hardness, fracture toughness and bending strength of $TiSi_2$–SiC and $TiSi_2$–SiC–Ti_3SiC_2 composites were tested at room temperature. The fracture toughness and bending strength of $TiSi_2$–SiC–Ti_3SiC_2 composites reach $5.4 \pm 0.3\,\mathrm{MPa{\cdot}m^{1/2}}$ and 700 ± 50 MPa, respectively. The factors leading to the improvement of the mechanical properties were discussed.

(Received October 24, 2005; Accepted December 16, 2005; Published March 15, 2006)

Keywords: *$TiSi_2$–SiC–Ti_3SiC_2, microstructure, mechanical properties, spark plasma sintering*

1. Introduction

In last ten years, advanced material systems for high temperature application based on refractory intermetallic compounds have been extensively investigated.[1,2] Among various classes of these intermetallic systems, titanium silicides have been identified as potential high temperature structural materials due to their superior combination of high melting point, oxidation resistance, and mechanical and microstructural stability. $TiSi_2$ is one of the most important titanium silicides. Besides the properties mentioned above, it has relatively high thermal and electrical conductivities that make it candidate for diffusion barriers and electronic interconnection applications.[3] The relatively low hardness makes the material easy to be machined. However, as in the case of many intermetallic compounds, the application of $TiSi_2$ compound is still greatly restricted by the low fracture toughness (about $2.2\,\mathrm{MPa\,m^{1/2}}$ for pure $TiSi_2$) and low bending strength (about 170 MPa for pure $TiSi_2$).[4] A promising alternative method is to produce a $TiSi_2$ matrix composite.

In Ti–Si–C system, there are many important compounds. SiC is a good candidate for reinforcement because it has high hardness, good high temperature strength and oxidation resistance. Li *et al.* synthesized $TiSi_2$–SiC composites by hot pressing Ti, Si and TiC powders with an enhancement of mechanical properties as compared to pure $TiSi_2$.[5] Nowadays Ti_3SiC_2 received much attention because of its unique combination of metallic and ceramic properties, such as good electrical conductivity, relatively high fracture toughness, good oxidation resistance and high temperature strength.[6,7] These properties ensure it suitable as the reinforcement component in ceramic-based composite.[8,9] Wang *et al.* synthesized Ti_5Si_3–TiC–Ti_3SiC_2 nanocomposite in which TiC and Ti_3SiC_2 were the dispersive phases for reinforcements.[10] However, TiC doesn't possess good high temperature oxidation resistance, which will decrease the high temperature oxidation resistance and strength of the composites. SiC is good substitute of TiC because of its good high temperature strength and oxidation resistance. So it is interesting to fabricate SiC and Ti_3SiC_2 reinforced $TiSi_2$–SiC–Ti_3SiC_2 composites.

Spark plasma sintering (SPS) technique is a new process with the advantages of rapid heating speed and short sintering time. Especially the short sintering period is advantageous in suppressing exaggerated grain growth. SPS has been used for fabricating a lot of kinds of ceramics, metal and biomaterials, such as Al_2O_3, Ti_3SiC_2, TiC–SiC, TiNi and hydroxyapatite.[11–15] In this work, $TiSi_2$–SiC and $TiSi_2$–SiC–Ti_3SiC_2 composites were *in situ* synthesized by spark plasma sintering to strengthen the $TiSi_2$.

2. Experimental Procedure

Commercially available C, Si and TiC were used as the starting powders. The mean particle sizes of C, Si and TiC were 9, 75 and 1.47 μm, respectively. The Si:TiC:C molar ratios of 6:2:0 and 6:4:1 were chosen as the starting compositions, marked as composition 1 and composition 2, respectively. They were blended in ethanol in Planet Ball Milling Machine for 12 h with agate media. After drying at 70°C for 12 h, the blended powders were screened through a 200-mesh sieve. Then the samples were sintered in a SPS apparatus (Sumitomo Coal Mining Co., Tokyo, Japan) under uniaxial pressure of 60 MPa in vacuum (below 6 Pa). The heating rate was controlled in the range of $150–200^\circ\mathrm{C{\cdot}min^{-1}}$. The sintering temperature was held at 1000, 1100, 1200 and 1260°C respectively for dwelling 5 min.

The densities of the resultant samples were measured according to the Archimedes's method. The crystalline phases were characterized by X-ray diffractometer (Rigaku: D/max 2200PC) with CuKα radiation. Field emission scanning electron microscopy (FESEM) and transmission electron microscopy (TEM) equipped with energy-dispersive spectroscopy (EDS) were employed to examine the microstructure. The hardness and fracture toughness of the samples

*Corresponding author, E-mail: cld@mail.sic.ac.cn

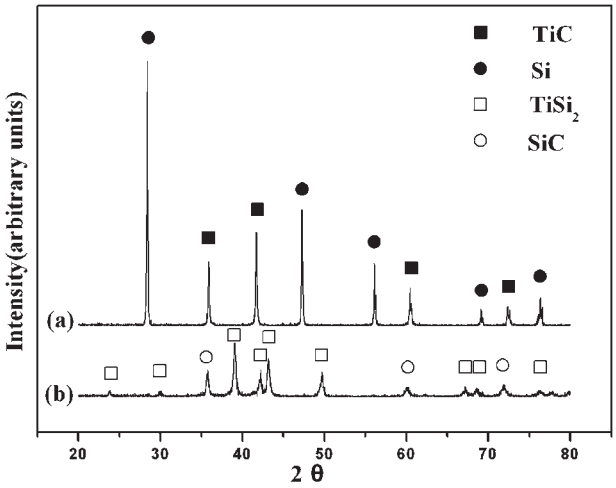

Fig. 1 XRD patterns of composition 1: (a) starting powder (b) $TiSi_2$–SiC composite.

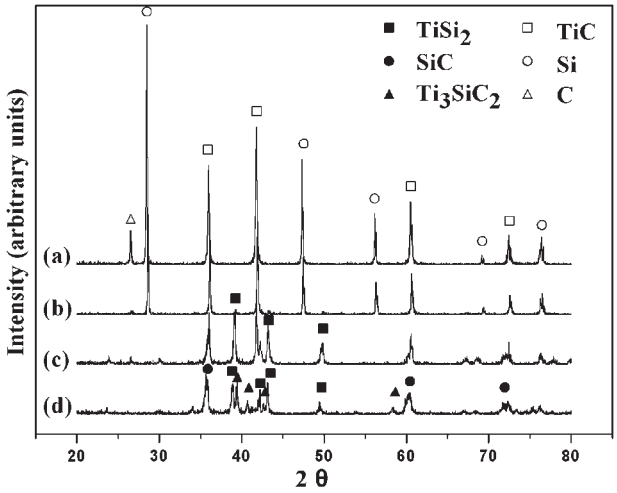

Fig. 2 XRD patterns of composition 2 sintered at different temperatures: (a) starting powder, (b) sintered at 1000°C, (c) sintered at 1100°C and (d) sintered at 1260°C.

were measured at room temperature by the Vickers diamond indentation method under a load of 49 N and a dwell of 10 s. The fracture toughness (K_{IC}) values were calculated using the following expression:[16)]

$$K_{IC} = P(\pi b)^{-3/2}(\mathrm{tg}\,\beta)^{-1},$$

where P is the Vickers load, b is the average length of cracks, and β is 68°. Three-point bending tests were performed to determine the strength using an Instron-5566 type of universal testing machine. The samples used in the bending tests were rectangular bars of 3 × 2 × 18 mm. The speed of crosshead displacement was 0.5 mm·min^{-1} with the span of 12 mm.

3. Results and Discussions

3.1 Microstructure

Figures 1(a) and (b) are the X-ray diffraction patterns of the starting powder and the resultant product of composition 1, respectively. Figure 1(b) shows that the sample consisted of $TiSi_2$ as a major phase coexisting with SiC phase without other phases, indicating that $TiSi_2$–SiC composite could be *in-situ* fabricated by spark plasma sintering according to following reaction [eq. (1)]:

$$3Si + TiC \rightarrow TiSi_2 + SiC \tag{1}$$

However, $TiSi_2$–SiC–Ti_3SiC_2 composite could not be fabricated only by using Si and TiC as reactants even the sintering temperature was as high as to 1260°C. C powder was added to the starting powders of Si and TiC. Figure 2 shows the X-ray diffraction patterns of the samples of composition 2 sintered at different temperatures. After sintered at 1000°C for 5 min, the constituents of the sample are the same with those of the starting powder indicating that reaction didn't begin at 1000°C. After sintered at 1100°C for 5 min, the diffraction peaks of Si disappeared and those of both $TiSi_2$ and SiC appeared. At the same time, the intensity of diffraction peaks of C and TiC became weak, indicating that reaction between Si and TiC occurred at this temperature. Fig. 2(d) is the diffraction spectrum of the sample sintered at 1250°C with dwelling time of 5 min. The diffraction peaks of Ti_3SiC_2 existed except those of $TiSi_2$ and SiC. It indicated that part of $TiSi_2$ reacted with TiC and C to form Ti_3SiC_2 as eq. (2):

$$TiSi_2 + 2TiC + C \rightarrow Ti_3SiC_2 + SiC \tag{2}$$

From these results, it can be concluded that the ternary composites should be formed through a two-step reaction process. Firstly, Si reacts with TiC at about 1100°C, and then part of $TiSi_2$ reacts with TiC and C to form Ti_3SiC_2 above 1100°C.

And the whole reaction should be [eq. (3)]:

$$6Si + 4TiC + C \rightarrow TiSi_2 + 3SiC + Ti_3SiC_2 \tag{3}$$

Figures 3(a) and (b) show the backscattered SEM images of polished surfaces of composition 1 and composition 2, respectively. The SiC particles (dark area) distributed uniformly in the composite. The dark spots in Fig. 3 were the SiC-rich areas rather than single SiC crystals. The white area is the mixture of $TiSi_2$ and Ti_3SiC_2 in Fig. 3(b). It is difficult to distinguish Ti_3SiC_2 from $TiSi_2$ only by the back scattered image.

Figure 4 shows the TEM images of grains of $TiSi_2$–SiC [Fig. 4(a)] and $TiSi_2$–SiC–Ti_3SiC_2 [Fig. 4(b)] samples. In Fig. 4(a), the SiC grains with grain size of 200–300 nm mainly disperse on the $TiSi_2$ grain boundaries. A lot of strain stripes emerge in Fig. 4(a) because of the thermal mismatching between $TiSi_2$ and SiC. There are some Ti_3SiC_2 plates confirmed by electron diffraction in composition 2 as shown in Fig. 4(b). The length of Ti_3SiC_2 grain is more than 1 μm and every Ti_3SiC_2 grain contains several layers. Ti_3SiC_2 grains have dominant (0001) facets because they grow most easily along the directions present within the basal plane. So Ti_3SiC_2 usually has a layered crystalline structure and the morphology of grains appears to be plate.

3.2 Mechanical properties

The hardness, fracture toughness and bending strength values listed in Table 1 are the average data of 6 tests. The

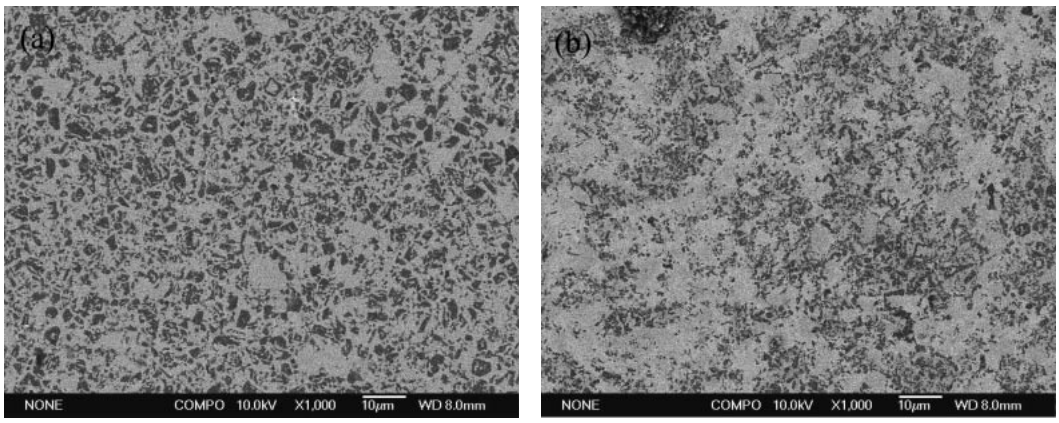

Fig. 3 Back scattered electron images of polished surface: (a) $TiSi_2$–SiC and (b) $TiSi_2$–SiC–Ti_3SiC_2.

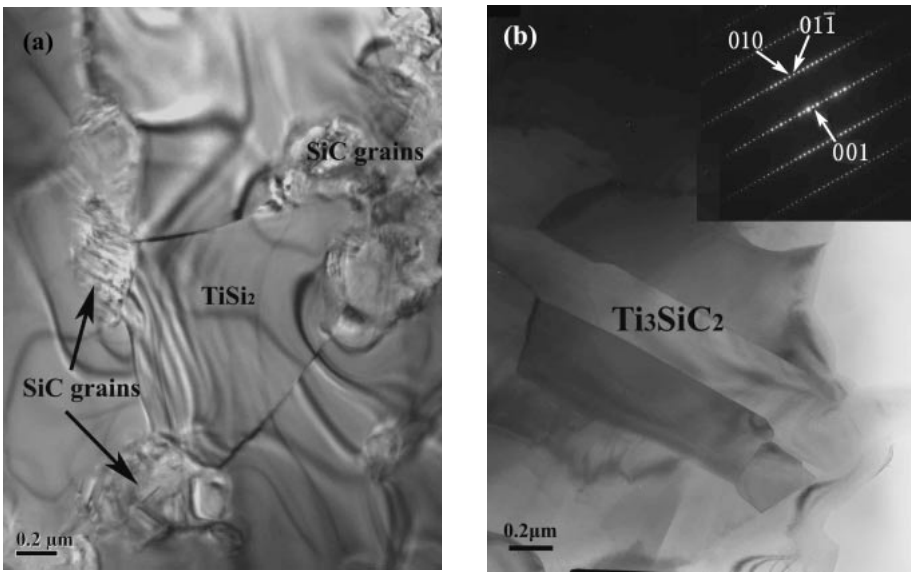

Fig. 4 TEM micrographs of $TiSi_2$–SiC and $TiSi_2$–SiC–Ti_3SiC_2 composites: (a) morphology of $TiSi_2$ and SiC in composition 1 and (b) morphology and electron diffraction of Ti_3SiC_2 in composition 2.

Table 1 Mechanical properties of specimens.

Specimen	Vickers microhardness, Hv (GPa)	Fracture toughness K_{IC} (MPa m$^{1/2}$)	Bending strength σ_b (MPa)
Sample 1	11.5 ± 0.3	3.3 ± 0.2	400 ± 50
Sample 2	12.1 ± 0.2	5.4 ± 0.3	700 ± 60

fracture toughness values of $TiSi_2$–SiC and $TiSi_2$–SiC–Ti_3SiC_2 reach 3.3 ± 0.2 MPa·m$^{1/2}$ and 5.4 ± 0.3 MPa·m$^{1/2}$, which are 150 and 250% higher than that of monolithic $TiSi_2$ (2.2 MPa m$^{1/2}$).[4)]

The improvement in fracture toughness for $TiSi_2$–SiC and $TiSi_2$–SiC–Ti_3SiC_2 composites was possibly attributed to the combination of crack deflection and crack bridging mechanisms. When the crack meets the dispersed SiC particles, it deflects and part of it propagates through the SiC particles. As we know, Young's modulus, thermal expansion coefficient and chemical compatibility of the matrix and second phase particles affect the properties of the composite. Because the thermal expansion coefficient of $TiSi_2$ ($\alpha_{TiSi_2} = 10 \times 10^{-6}$ K^{-1}) is larger than that of SiC ($\alpha_{SiC} = 4.8 \times 10^{-6}$ K^{-1}), hydrostatic compressive stress appears in the second phase (SiC). At the same time, there will be radial compressive stress and tangential tensile stress in the matrix around the SiC particles. If the SiC locates on the crack extension plane, the crack will firstly reach the boundary of the $TiSi_2$ and SiC grains. The surface energy of SiC grains is much larger than the interface fracture energy of $TiSi_2$/SiC interface. So the crack tends to bypass the SiC particles and propagate along the $TiSi_2$/SiC interface. However, sometimes the crack drills through the particles if the particles are irregular. As the TEM image shows, the size of the SiC is in the range of 200–300 nm, so the effect of the crack deflection on the improvement of fracture toughness was weakened. When the crack extension direction is not parallel to the priority growth direction of Ti_3SiC_2, the crack will propagate along the interface between matrix and Ti_3SiC_2. Because the length of the Ti_3SiC_2 grain is more than 1 μm, the effect of the crack bridging on the improvement of fracture toughness is remarkable. Figure 5 is the back scattered images of typical trajectories of indentation crack extension of composition 2.

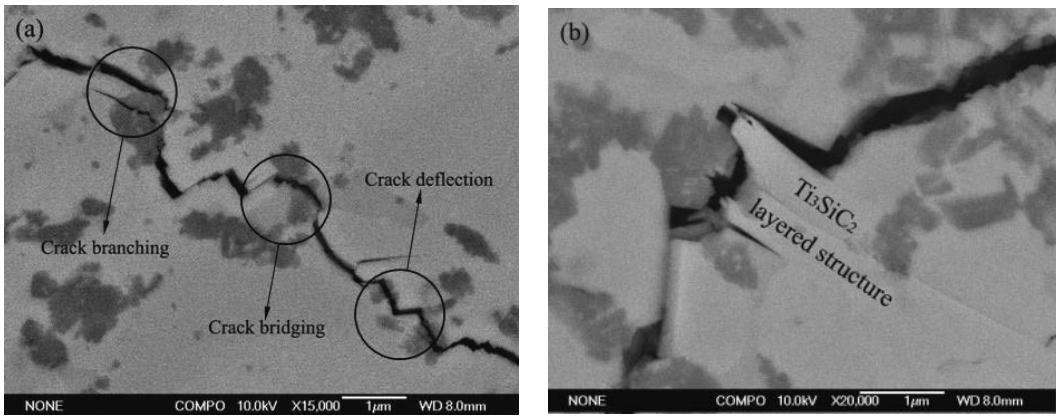

Fig. 5 Back scattered electronic images of crack propagation in the composition 2 showing: (a) crack bridging, crack branching and crack deflection and (b) crack bridging of Ti_3SiC_2.

In the course of the crack propagation in Fig. 5(a), crack branching, crack bridging and crack deflection can be observed at the same time. At some points, the crack propagated in a zigzag fashion or deflected at a vertical angle. Crack deflection of this degree is very rare in common ceramic.[17] It can be found clearly that the layered Ti_3SiC_2 grain was pulled out from the $TiSi_2$ matrix in Fig. 5(b). The crack bridging of Ti_3SiC_2 mainly contributes to the improvement of the fracture toughness of TiS_2–SiC–Ti_3SiC_2.

The bending strength values of $TiSi_2$–SiC and $TiSi_2$–SiC–Ti_3SiC_2 composite reach 450 ± 50 and 700 ± 60 MPa, which are much higher than that of monolithic $TiSi_2$ (170 MPa). Figure 3 shows that the microstructure of $TiSi_2$–SiC–Ti_3SiC_2 is finer than that of $TiSi_2$–SiC composite, which in some extent led to the enhancement of the bending strength. Besides grain size, grain shape could affect the strength of materials as well. It was believed that better contact or joint could form between the long grains, which could improve the fracture strength of grains. Wang *et al.* utilized rodlike β-Si_3N_4 crystal to strengthen $MoSi_2$ matrix and effectively improved the flexural strength and fracture toughness.[18] In bending tests, the crack propagation experienced a course which was similar with the crack spread in indentation tests. So the crack bridge aroused by layered Ti_3SiC_2 also contributed to the improvement of bending strength.

4. Conclusion

In this work, $TiSi_2$–SiC–Ti_3SiC_2 composites were successfully *in-situ* fabricated using TiC, Si and C particles in micrometer as starting reactants. The microstructure characterization results showed that *in-situ* synthesized SiC grains with grain size of 200–300 nm mainly dispersed on the $TiSi_2$ grain boundaries. The fracture toughness has been shown to increase from $3.3 \pm 0.2\,\mathrm{MPa{\cdot}m^{1/2}}$ for $TiSi_2$–SiC composite up to $5.4 \pm 0.3\,\mathrm{MPa{\cdot}m^{1/2}}$ for the $TiSi_2$–SiC–Ti_3SiC_2 composite. And the bending strength was improved from 450 ± 50 MPa up to 700 ± 60 MPa. The improvement in fracture toughness was attributed to crack deflection and crack bridging resulted from nano-SiC particles and layered structural Ti_3SiC_2 grains. The introduction of layered Ti_3SiC_2 also improved the bending strength of the composites greatly.

Acknowledgements

We gratefully acknowledge the financial support by the Natural Science Foundation of China (Grant Nos. 50302012 and 50232020) and the Open Foundation of State Key Laboratory (No. SKL200504SIC).

REFERENCES

1) P. J. Meschter and D. S. Scgwartz: J. Met. **41** (1989) 52–55.
2) A. K. Bhattacharya: J. Am. Ceram. Soc. **74** (1991) 2707–2711.
3) W. Y. Yang, H. Iwakuro, H. Yagi, T. Kuroda and S. Nakamura: Jpn. J. Appl. Phys. **23** (1984) 1560–1567.
4) R. Rosenkranz and G. Frommeyer: Mater. Sic. Eng. A **152** (1992) 288–294.
5) J. L. Li, D. L. Jiang and S. H. Tan: J. Eur. Ceram. Soc. **20** (2000) 227–233.
6) T. Okana, T. Yano and T. Iseki: Trans. Met. Soc. Jpn. **14A** (1993) 597–600.
7) C. Racault, F. Langlais and R. Naslain: J. Mater. Sci. **29** (1994) 3384–3392.
8) M. W. Barsoum and T. El-Raghy: J. Electrochem. Soc. **144** (1997) 2508–2512.
9) R. Radhakrishnan, J. J. Williams and M. Akine: J. Alloys Compd. **285** (1999) 85–88.
10) L. J. Wang, W. Jiang, L. D. Chen and G. Z. Bai: J. Mater. Res. **19** (2004) 3004–3008.
11) S. W. Wang, L. D. Chen, T. Hirai and J. K. Guo: J. Mater. Res. **16** (2001) 3514–3519.
12) Z. F. Zhang, Z. M. Sun, H. Hashimoto and T. Abe: J. Eur. Ceram. Soc. **22** (2002) 2957–2961.
13) L. J. Wang, W. Jiang, L. D. Chen and S. Q. Bai: J. Am. Ceram. Soc. **87** (2004) 1157–1160.
14) Y. Q. Fu, S. Moochhala and C. Shearwood: Proc. SPIE Int. Soc. Opt. Eng. **5275** (2004) 9–17.
15) J. L. Xu, K. A. Khor, Y. W. Gu, R. Kumar and P. Cheang: Biomaterials **26** (2005) 2197–2207.
16) A. G. Evans and E. A. Charles: J. Am. Ceram. Soc. **59** (1976) 371–372.
17) J. F. Li, W. Pan, F. Sato and R. Watanabe: Acta Mater. **49** (2001) 937–945.
18) G. Wang, W. Jiang, G. Z. Bai and D. Y. Chen: Mater. Lett. **58** (2004) 308–311.